Supporting Information

Novel Fluorene-Based Copolymers Containing Branched 2-Methyl-Butyl Substituted Fluorene-Co-Benzothiadiazole Units for Remarkable Optical Gain Enhancement In Green-Yellow Emission Range

Zhou Yu, Xiangru Guo, Qi Zhang, Lang Chi,Ting Chen, Ruidong Xia,* Longfei Wu, Larry Lüer, Juan Cabanillas-Gonzalez*

Z. Yu, X. Guo, Q. Zhang, L. Chi, T. Chen, Prof. R. Xia
Key Laboratory for Organic Electronics and Information Displays (KLOEID) &
Institute of Advanced Materials (IAM), Jiangsu National Synergetic Innovation Center for Advanced Materials (SICAM), Nanjing University of Posts & Telecommunications, 9 Wenyuan Road, Nanjing 210023, China, E-mail: iamrdxia@njupt.edu.cn

L. Wu, Dr L. Lüer, Dr. J. Cabanillas-Gonzalez
Madrid Institute for Advanced Studies (IMDEA Nanociencia), Calle Faraday 9, Ciudad Universitaria de Cantoblanco, Spain, E-mail: juan.cabanillas@imdea.org

Polymer Synthesis:

20F1/4F8BT (polystyrene equivalent Mw = 35,920, polydispersity index = 2.1) consisted of 20% 9,9-di(2-methyl)butyl (F1/4) , 30% 9,9-dioctyl substituted fluorine (F8) units and 50% benzothiadiazole (BT) units. The Suzuki arenebisboronic ester/dibromoarene coupling route was used. This method yields statistical copolymers for which there need not be a predetermined sequence of F8/BT and F1/4/BT units but instead where variable length 'blocks' (sequences of repeating F1/4/BT units or F8/BT units) could be presented in the backbone structure. PFO was purchased with typical polystyrene equivalent molecular weight Mw = 150,000- 160,000.
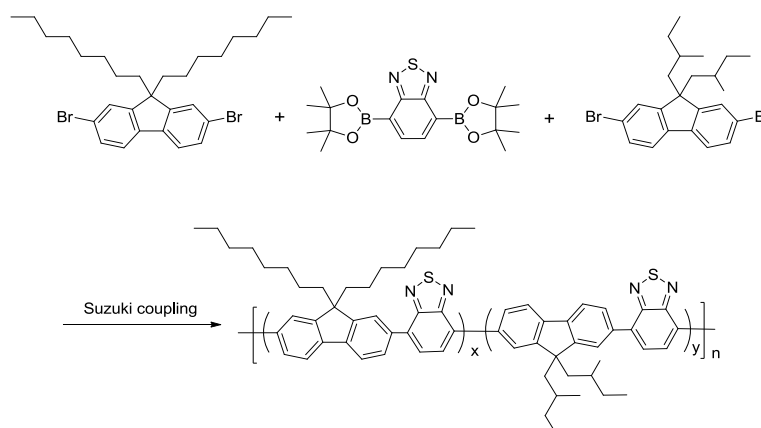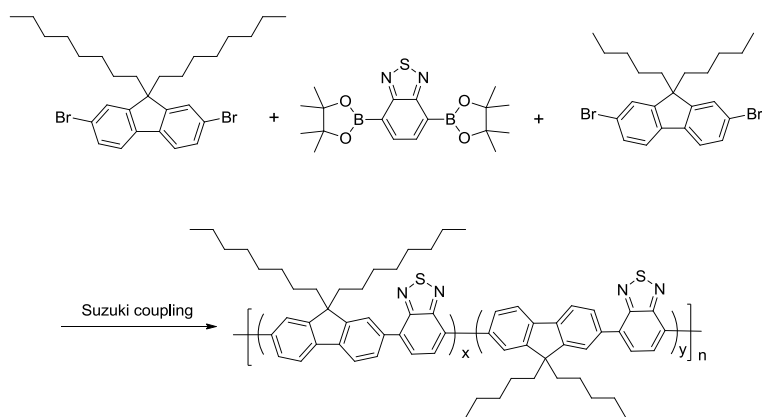
Scheme S1

Table S1. Properties of copolymers

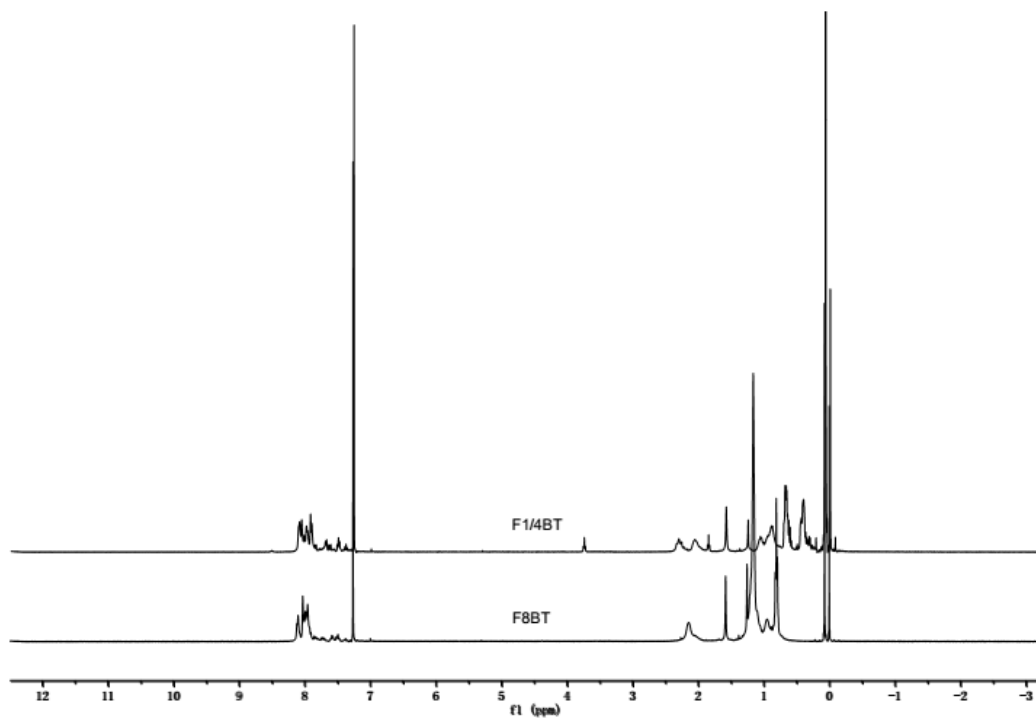| Polymer	Molar ratio F8 : F1/4(F5) : BT	Mn	Mw	PDI	PLQE (± 10%)
20F1/4F8BT	3:2:5	17 086	35 920	2.10	0.37
15F1/4F8BT	3.5:1.5:5	12 242	29 174	2.38	0.32
10F1/4F8BT	4:1:5	15 244	37 829	2.48	0.26
F1/4BT	0:1:1	5 088	9 356	1.83	0.14
F8BT	1:0:1	12 544	28 398	2.26	0.32
20F5F8BT	3:2:5	8622	22632	2.62	—

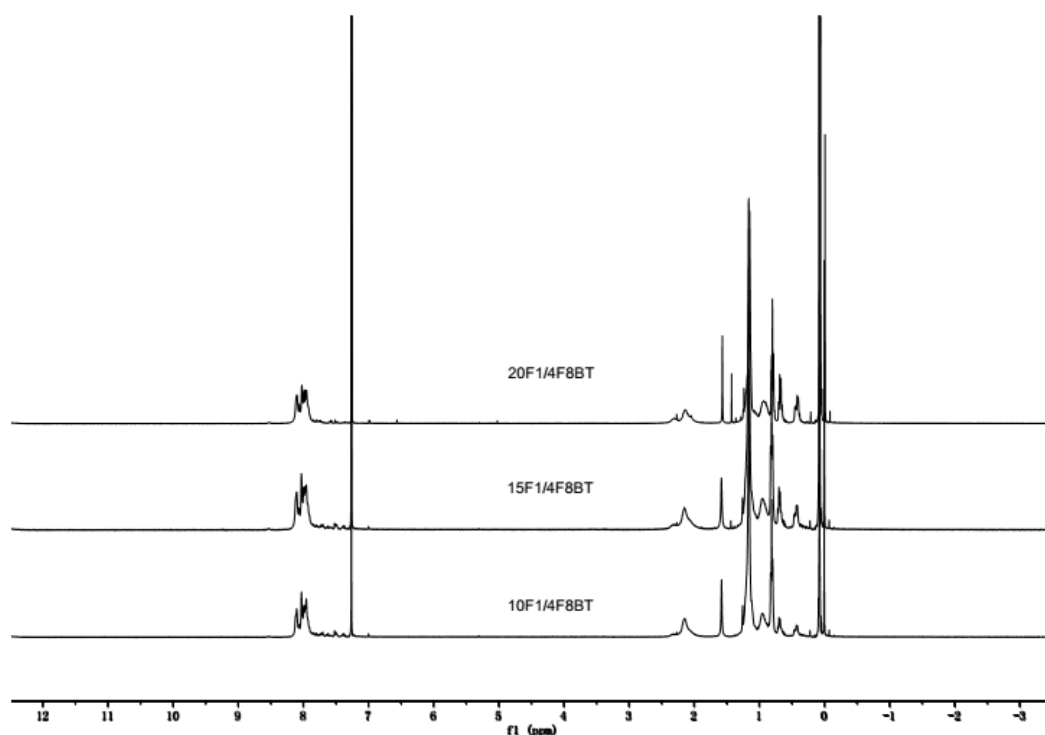**Figure S1.** Comparison of ^{1}H NMR spectrum of F1/4BT and F8BT

Figure S2. Comparison of ^{1}H NMR spectrum of 10F1/4F8BT, 15F1/4F8BT and 20F1/4F8BT

Materials: The manipulations involving air-sensitive reagents were performed in an atmosphere of dry N_2. The chemicals and solvents, unless otherwise specified, were purchased from Aladdin, Aldrich or Acros, and used without further purification.

Characteristic Methods: ^{1}H and ^{13}C-nuclear magnetic resonance (NMR) spectra were recorded on a Bruker Ultra Shied Plus 400 MHz instrument with *d*-CDCl$_3$ as the solvent and tetramethylsilane (TMS) as the internal standard. The quoted chemical shifts are in *ppm* and the *J* values are expressed in Hz. The splitting patterns have been designed as follows: s (singlet), d (doublet), t (triplet), dd (doublet of doublets), and m (multiplet).

Monomer Synthesis. The synthesis steps for preparation of the monomers are described at bellow and outlined in Scheme S2.
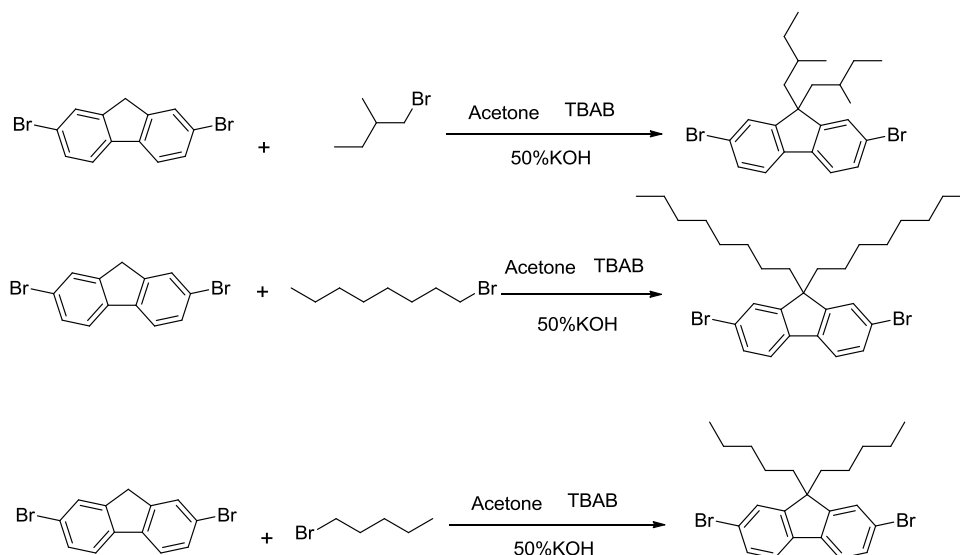
Scheme S2. The synthetic route of the monomers.

The synthesis of 2,7-dibromo-9,9-dioctylfluorene (F8) and 2,7-dibromo-9,9-di(2-methyl)

butylfluorene (F1/4), 2,7-dibromo-9,9-dipentylfluorene (F5)

To a solution of 2,7-dibromo-fluorene (4.86 g, 15 mmol) and Tetrabutylammonium bromide

(TBAB) in acetone (30 ml) was added a solution of 50%KOH (10.6 mL, 91.8 mmol). After

the 1-Bromooctane (10.13 g, 52.5 mmol) was added to the mixed solution, the reaction was

heated at reflux and stirred overnight. Then the solvent was removed and the organic layer

was washed with water and extracted with dichoromethane (CH_2Cl_2, 3×100 ml) for three

times. The combined organic layers were collected, dried over anhydrous sodium sulphate

(Na_2SO_4), filtered and evaporated to remove the solvent. The crude oil product of 2,7-

dibromo-9,9-dioctylfluorene was further purified by flash column chromatography on silica

gel (200-300 mesh). Recrystallize several times from hexane to afford the pure compounds of

F8. Yield: 7.40 g of white solid (90%). ^{1}H NMR (400 MHz, CDCl$_3$, *ppm*): δ 7.55 − 7.49 (m,

2H), 7.46 (dd, *J* = 6.6, 1.8 Hz, 4H), 1.96 − 1.87 (m, 4H), 1.35 − 0.86 (m, 24H), 0.83 (t, *J* = 7.1

Hz, 6H). ^{13}C NMR (100 MHz, CDCl$_3$, *ppm*) 152.55 , 139.08 , 130.16 , 126.17 , 121.50 ,

121.16 , 55.70 , 40.20 , 31.72 , 29.90 , 29.22 , 23.64 , 22.68 , 14.17. GC-MS: m/z calcd for

$C_{29}H_{40}Br_2$ [M+H]$^+$: 548.44; found: 548.

To a solution of 2,7-dibromo-fluorene (4.86 g, 15 mmol) and Tetrabutylammonium bromide (TBAB) in acetone (30 ml) was added a solution of 50%KOH (10.6 mL, 91.8 mmol). After the 1-Bromo-2-methylbutane (7.92 g, 52.5 mmol) was added to the mixed solution, the reaction was heated at reflux and stirred overnight. Then the solvent was removed and the organic layer was washed with water and extracted with dichoromethane (CH_2Cl_2, 3×100 ml) for three times. The combined organic layers were collected, dried over anhydrous sodium sulphate (Na_2SO_4), filtered and evaporated to remove the solvent. The crude oil product of 2,7-dibromo-9,9-di(2-methyl)butylfluorene was further purified by flash column chromatography on silica gel (200-300 mesh). Recrystallize several times from hexane to afford the pure compounds of F5. Yield:5.92 g of white solid (85%). ^{1}H NMR (400 MHz, CDCl$_3$, ppm): δ 7.56 − 7.43 (m, 6H), 2.05 (ddd, J = 13.9, 9.8, 4.0 Hz, 2H), 1.88 − 1.77 (m, 2H), 0.99 − 0.73 (m, 4H), 0.71 − 0.52 (m, 8H), 0.28 (dd, J = 14.5, 6.7 Hz, 6H). ^{13}C NMR (100 MHz, CDCl$_3$, ppm) 152.95 , 139.13 , 130.18 , 127.14 , 121.14 , 55.19 , 47.74 , 30.98 , 30.58 , 20.96 , 10.93. GC-MS: m/z calcd for $C_{23}H_{28}Br_2$ [M+H]$^+$: 464.28; found: 464.

To a solution of 2,7-dibromo-fluorene (4.86 g, 15 mmol) and Tetrabutylammonium bromide (TBAB) in acetone (30 ml) was added a solution of 50%KOH (10.6 mL, 91.8 mmol). After the 1-bromopentane (7.92 g, 52.5 mmol) was added to the mixed solution, the reaction was heated at reflux and stirred overnight. Then the solvent was removed and the organic layer was washed with water and extracted with dichoromethane (CH_2Cl_2, 3×100 ml) for three times. The combined organic layers were collected, dried over anhydrous sodium sulphate (Na_2SO_4), filtered and evaporated to remove the solvent. The crude oil product of 2,7-dibromo-9,9-dipentylfluorene was further purified by flash column chromatography on silica gel (200-300 mesh). Recrystallize several times from hexane to afford the pure compounds of F5. Yield:6.28 g of white solid (90%). ^{1}H NMR (400 MHz, CDCl$_3$, ppm): δ 7.55 − 7.50 (m, 2H), 7.45 (dq, J = 3.1, 1.7 Hz, 4H), 1.97 − 1.88 (m, 4H), 1.14 − 1.01 (m, 8H), 0.73 (t, J = 6.8

Hz, 6H), 0.65 – 0.53 (m, 4H). ^{13}C NMR (100 MHz, CDCl$_3$, ppm) δ 152.56, 139.08, 130.17, 126.17, 121.50, 121.16, 55.69, 40.18, 32.11, 23.36, 22.29, 14.00. GC-MS: m/z calcd for C$_{23}$H$_{28}$Br$_2$ [M+H]$^+$: 464.28; found: 464.

4,7-bis(4,4,5,5-tetramethyl-1,3,2-dioxaborolan-2-yl)benzo[1,2,5]thiadiazole (BT) was purchased, and texted as the monomers above. ^{1}H NMR (400 MHz, CDCl$_3$, ppm) δ 8.13 (s, 2H), 1.44 (s, 24H). ^{13}C NMR (100 MHz, CDCl$_3$) δ 156.95 (s), 137.81 (s), 84.45 (s), 24.91 (s). GC-MS: m/z calcd for C$_{23}$H$_{28}$Br$_2$ [M+H]$^+$: 388.10; found: 388.

Measurement

UV-Visible Absorption (UV) and Photoluminescence (PL). Ultraviolet-visible (UV-Vis) spectra were recorded on an UV-3600 Shimadzu UV-VIS-NIR spectrophotometer, while fluorescence spectra were obtained using an RF-5301PC spectrofluorophotometer with a Xenon lamp as light source.
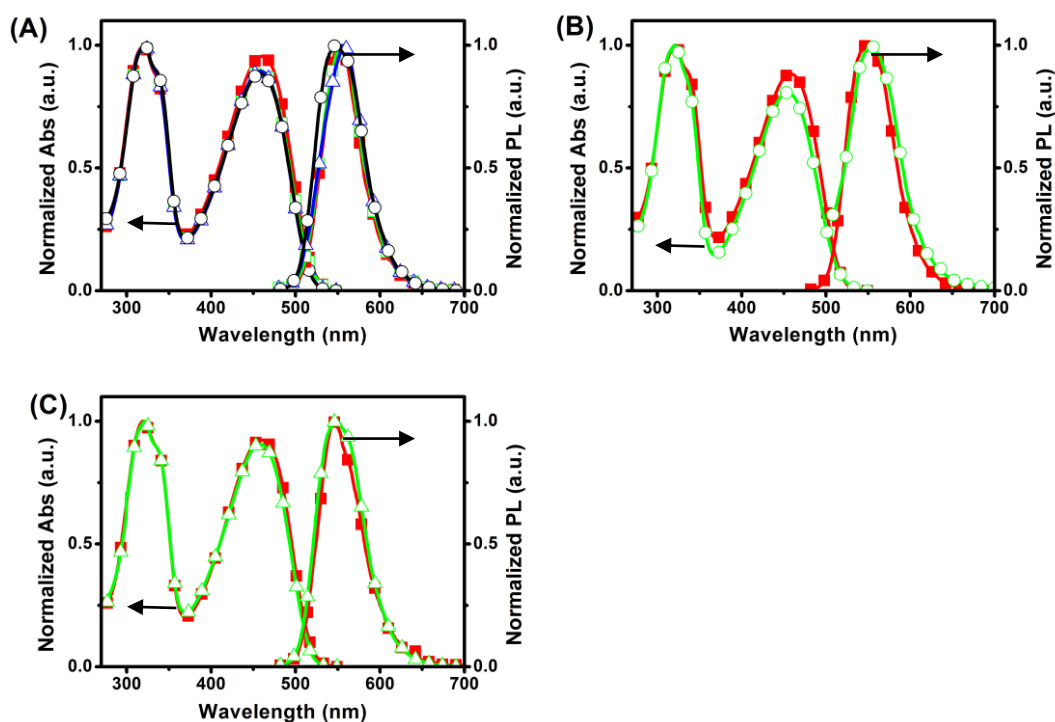

Figure S3. Normalized absorbance and photoluminescence spectrum of (**A**) F8BT (open circles), 10F1/4F8BT (open triangles), 15F1/4F8BT (open squares), and 20F1/4F8BT (filled squares). (**B**) 20F5F8BT (open circles) and F8BT (filled squares). (**C**) HF8BT (high

molecular weight F8BT) (filled squares) and LF8BT (low molecular weight F8BT) (open triangles).

Electrochemical properties. Cyclic voltammogram measurements were performed at room temperature on a CHI660E system in a typical three-electrode cell with a working electrode (glass carbon), a reference electrode (Ag/Ag$^+$, referenced against ferrocene/ferrocenium (FOC)), and a counter electrode (Pt wire) in an acetonitrile solution of tetrabutylammonium hexafluorophosphate (Bu$_4$NPF$_6$) (0.1 M) at a sweeping rate of 100 mV s^{-1}. The highest occupied molecular orbital (HOMO) and the lowest unoccupied molecular orbital (LUMO) energy levels (E_{HOMO} and E_{LUMO}) of the materials are estimated based on the reference energy level of ferrocene (4.8 eV below the vacuum):

$$E_{HOMO} = -\left[E_{onset}^{Ox} - (0.34) \right] - 4.8 eV \qquad 1$$

$$E_{LUMO} = -\left[E_{onset}^{Red} - (0.34) \right] - 4.8 eV \qquad 2$$

where the value of 0.34 V is the onset oxidative voltage of FOC *vs* Ag/Ag$^+$ and E_{onset}^{Ox} and E_{onset}^{Red} are the onset potentials of the oxidation and reduction, respectively.

Table S2. Electrochemical properties of polymers thin solid films.

Copolymers	Eox (V)	Ered (V)	E_{HOMO} (-eV)	E_{LUMO} (-eV)	E_g (eV)
20F1/4F8BT	1.50	-0.70	5.96	3.76	2.20
15F1/4F8BT	1.51	-0.69	5.97	3.77	2.20
10F1/4F8BT	1.50	-0.70	5.96	3.76	2.20
F1/4BT	1.43	-0.73	5.89	3.73	2.26
F8BT	1.50	-0.83	5.96	3.63	2.33

ASE Tests. For ASE measurements, samples were optically pumped at wavelength of 390 nm with Q-switched, neodymium ion doped yttrium aluminium garnate [Nd3+: YAG] laser (Continum Surelite II-10) pumped, type-II β-BaB2O4 [BBO], optical parametric oscillator (Panther EX) that delivered 3 ns pulses at a repetition rate of 10 Hz. Output signals are

collected with a fiber-coupled grating spectrometer (Andor Co.) equipped with a CCD detector (Newton Co.). The size of narrow excitation strip is 550 μm x 4 mm.
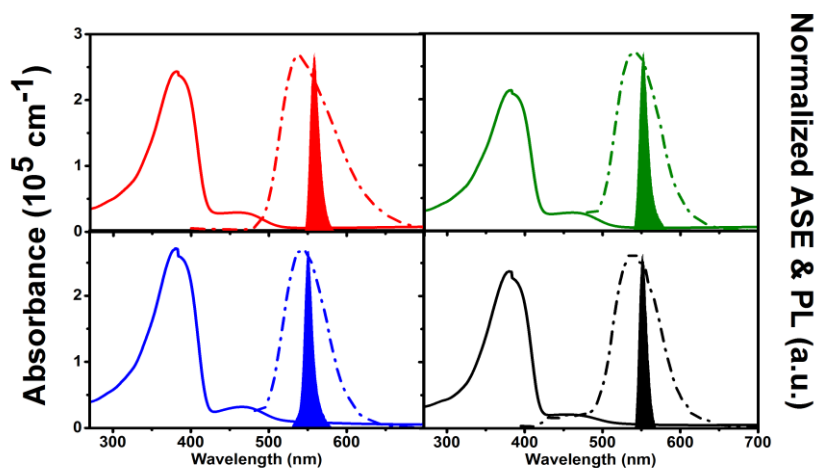

Figure S4. The comparison of UV absorbance (solid lines),, PL (dash dot lines) and ASE (filled lines) properties of PFO:20F1/4F8BT (**top left**) and PFO:15F1/4F8BT (**top right**), PFO:10F1/4F8BT (**down left**) and PFO:20F5F8BT (**down right**) blended films.
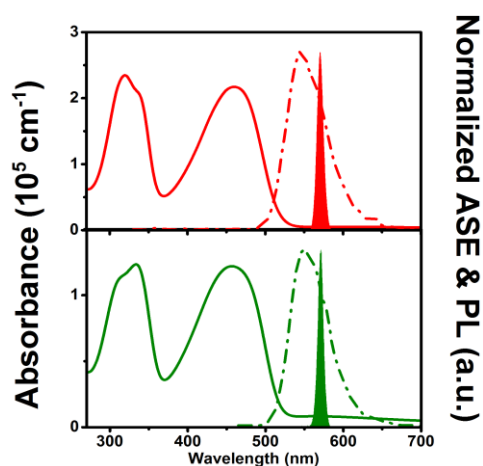

Figure S5. The comparison of UV absorbance (solid lines), PL (dash dot lines) and ASE (filled lines) properties of purchased F8BT film (**above**) and 15% (w.t.) F1/4BT/F8BT blended film (**below**).

PL decay study. The luminescence decay curves were measured using an Edinburgh FLSP920 fluorescence spectrophotometer equipped with a 375 nm laser (typical pulse width: 55 ps; pulse repetition frequencies: 20 MHz).
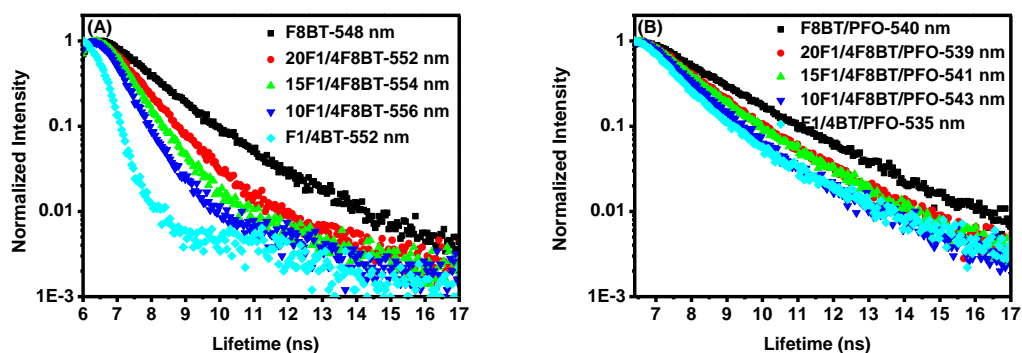

Figure S6. Emission intensity vs time measured at **(A)** F8BT (548 nm), 20F1/4F8BT (552 nm), 15F1/4F8BT (554 nm), 10F1/4F8BT (556 nm), F1/4BT (552 nm) after excitation at 450 nm and **(B)** the blend of PFO with F8BT (540 nm), 20F1/4F8BT (539 nm), 15F1/4F8BT (541 nm), 10F1/4F8BT (543 nm) and F1/4BT (535 nm) after excitation at 390 nm for PFO.

Quantum chemical calculations

Table S3 and Figure S7 present the proposed structures and calculated torsion angles between fluorene and BT units. The F1/4 and BT unit (37.65º) is higher than the one between F8 and BT unit (36.10º), and F5 (straight alkyl chains substituted fluorene) and BT unit (36.62º) as listed in Table S3. It can be seen how the bulky side-chain substituents of F1/4, is an essential factor causing steric hindrance. The introduction of F1/4 into F8BT leads to a change in dihedral angle in the copolymer skeleton. Moreover, the comparison of torsion angle between various fluorene units (bearing branched or straight alkyl chains) and the BT units also shows that branched substituted fluorene unit (37.54º) formed slightly higher torsion angle than the straight one (37.45º) with BT unit. These observations obtained from calculations proof that branch side-chain substitution leads to a slightly less planar backbone conformation.
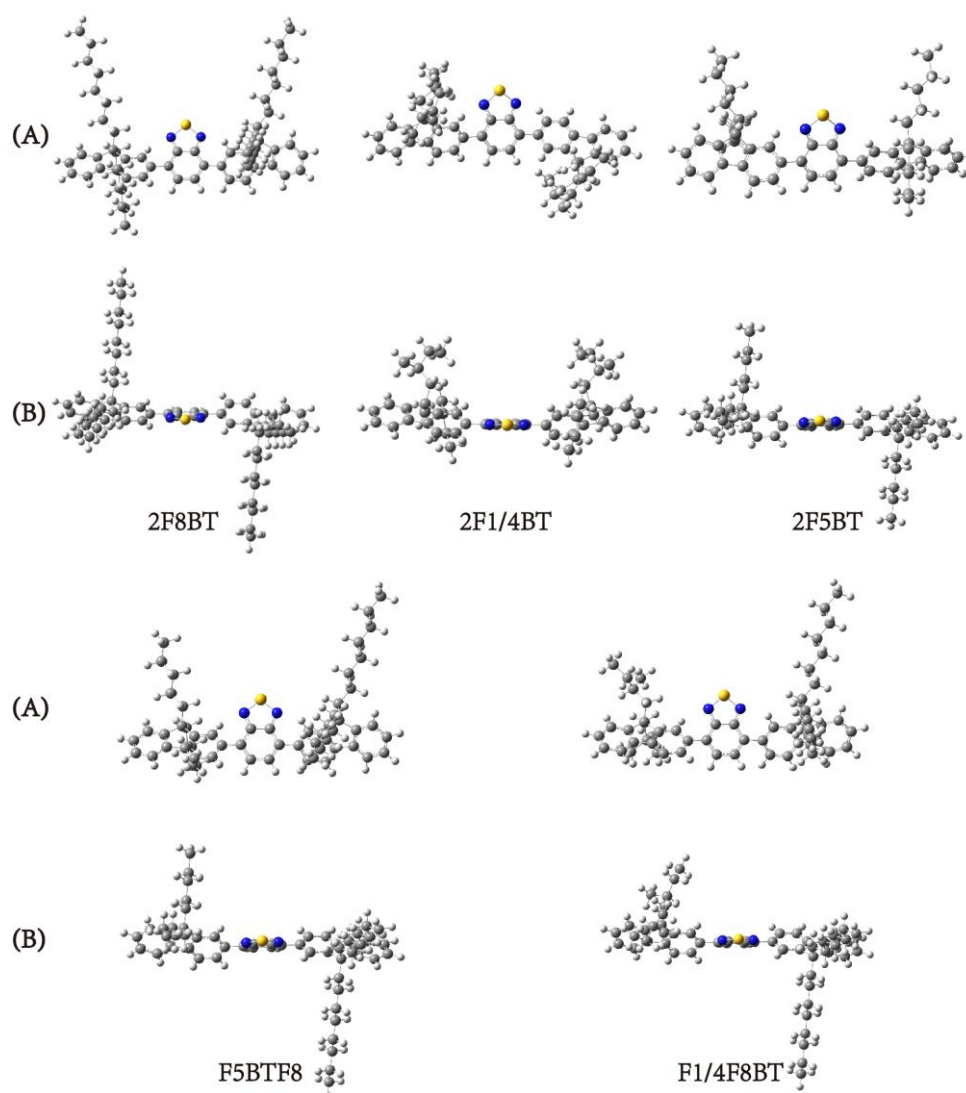
Figure S7. The calculated proposed structural units for F8BT and F1/4BT (F5BT). (A) Frontal views; (B) Vertical views.

Table S3. The calculated torsion angles between fluorene and BT units of several proposed structural units.

Polymer	torsion angle [L] (°)	torsion angle [R] (°)
2F8BT	36.10	36.10
2F1/4BT	37.65	37.65

2F5BT	36.62	36.62
F5BTF8	37.45	37.02
F1/4BTF8	37.54	37.22

[L] means the torsion angle between the left unit and the center unit. [R] means the torsion angle between the right unit and the center unit.

Modeling of transient absorption (TA) spectra

Transient absorption spectra have been measured at various intensities in order to obtain the densities of excitons in the donor and acceptor phase, to trace the efficiency of energy transfer from donor towards the acceptor and the presence of exciton annihilation in both phases. Furthermore, we needed to assess the density of polarons in both phases, because these are known to overlap with SE, inhibiting a net gain if too abundant. Due to spectral congestion, no probe energy can be found which is specific for any of these photoexcitations. Therefore, a technique called global fitting has been applied that has been described in detail by van Stokkum et al.[i] In short, the validity of Lambert Beer's law is assumed (system is far from total absorption at all probing energies):

$$A(t,w) = \sum_i c_i(t)\sigma_i(w) \qquad\qquad (\text{EQ. S1})$$

to reproduce the measured transient absorption spectrum A(t,w), which depends on time t and probe energy w), by a superposition of states I with characteristic time-resolved concentration $c_i(t)$ and energy-resolved absorption cross-section σ(w). Eq. S1 can be written in matrix form:

$$A = c \times \sigma \qquad\qquad (\text{EQ. S2})$$

In eq. S2, each column of the c matrix represents one complete concentration-time dependence of a state I, while each row of the σ matrix represents the full (time-invariant) spectrum of that state i.

In a first step, we use singular value decomposition (SVD) to find out how many states need to be considered in eq. S2. As Figs S8 and S10 show, at low intensity both acceptor materials can be modeled by two components, whereby the second one is one order of magnitude weaker and characterized by a first derivative like shape around the band maximum of the dominant state. The second state is therefore identified as a time-dependent shift of the first

state, rather than a different photoexcitation. We assign this to the singlet exciton; the shift is due to spectral relaxation after pumping at 387 nm. Only at higher intensity (Figs S9 and S11), we find the small presence of a dedicated third state around 2.4 eV, explained by polarons created by singlet annihilation. From these findings, we chose to assume one single state in eq. S2, namely the singlet exciton, for all TA spectra from the acceptor materials. For PFO, instead, we found the presence of two dedicated states, namely singlet excitons and polarons, which is also well known in the literature. Therefore we used two states to solve eq. S2 in the case of PFO.

The spectral shapes σ in eq. S2 were found iteratively by tuning appropriate lineshape functions (Voigt profiles to account for inhomogeneous broadening or skewed Gaussians to account for a Boltzmann type occupation of available states. The lineshape function were considered as converged if they fitted a complete set of experiments at all times and pump intensities. Then eq. S2 is used with the optimized lineshape functions to obtain the desired relative concentrations. The resulting global fits are shown in Fig. S14-S16 (only part of the globally fitted TA spectra is shown).

In a final step, the lineshape functions optimized in the pure materials are used to fit the TA spectra for the blended materials. In doing so, we assume that only the photoexcitation dynamics but not the optical probes change upon blending. The goodness of the resulting global fits (Fig. S17 and S18) partly justifies this assumption although a final proof would have to come from a dedicated study globally fitting TA spectra across a large range of blending ratios. From the areas underneath the isolated spectra for singlets and polarons (thin black and red curves, respectively, in Figs 14-18) we directly obtain the relative concentration that we display in Fig.6 of the main text.

Calculation of absolute concentrations of excited states

The spectral modeling, as described above, yields time-resolved spectral weights, which are the areas under the curves associated with each excited state considered in the spectral model. We can use these spectral weights

$$a_i(t) = \int_\omega A_i(\omega, t) d\omega \qquad\qquad \text{(EQ. S3)}$$

to calculate the time-resolved concentrations of all photoexcitations {i} present in the system. To this end, we restate eq. (S1) for a single photoexcitation.

$$A_i(t, \omega) = d \cdot c_i(t) \cdot \sigma_i(\omega) \tag{EQ. S4}$$

Integrating over all probe energies ω yields

$$\int_\omega A_i(t, \omega)d\omega = d \cdot c_i(t) \cdot \int_\omega \sigma_i(\omega)d\omega \tag{EQ. S5}$$

such that for the time-resolved concentration of photoexcitation i:

$$c_i(t) = \frac{\int_\omega A_i(t,\omega)d\omega}{d \cdot \int_\omega \sigma_i(\omega)d\omega} \tag{EQ. S6}$$

From the spectral modeling, we obtain the time-resolved spectral weights:

$$a_i(t) = \int_\omega A_i(t, \omega)d\omega \tag{EQ. S7}$$

Letting

$$\alpha_i = \int_\omega \sigma_i(\omega)d\omega \tag{EQ. S8}$$

which is related to the oscillator strength f of a certain transition and can in principle be calculated, we obtain:

$$c_i(t) = \frac{a_i(t)}{d\alpha_i} \tag{EQ. S9}$$

In the absence of any relaxation (at t = 0, assuming that there are no relaxation processes that are faster than our instrumental time resolution of about 150 fs), the total concentration must equal the concentration of absorbed photons:

$$c_{tot} = c_{ph} = \frac{1}{d}\sum_i \frac{a_i(0)}{\alpha_i} \tag{EQ. S10}$$

Here, the concentration of absorbed photons is given by:

$$c_{ph} = \frac{n_{\widetilde{ph}}}{d} = \frac{2N_{ph}(1-T)}{Ad} = 2\frac{N_{ph}}{\pi w_{pu}^2 \cdot d} = \frac{2E_{pu}/E_{ph}}{\pi w_{pu}^2 \cdot d} \tag{EQ. S11}$$

Here, $n_{\widetilde{ph}}$ is the density of absorbed pump photons per unit area at the position of the probe pulseA , N_{ph} is the number of absorbed photons, T is the transmission of the sample at the deployed pump wavelength assuming no scattering and reflection losses, A is the effective area of the pump spot, assumed Gaussian, w_{pu} is the Gaussian spot size of the pump pulse, E_{pu} is the total energy of a single pump pulse, E_{ph} is the energy of a single photon at the wavelength of the pump pulse. The factor 2 in the last fraction comes in by assuming that the probe pulse spot sits in the center of the pump pulse with a spot size $w_{pr} \ll w_{pu}$. These assumptions are all approximately justified in our experiment.

The relative oscillator strengths α_i can in principle be obtained by seeking experimental situations in which the ratios $a_i(0)/c_{tot}$ change, which allows to find them by solving the

resulting system of linear equations (different pump intensity, wavelength, sample composition, etc.). Another possibility is to relate the excited state oscillator strengths with those of the corresponding ground state bleach, which can be known by measuring the absorption spectrum of a known amount of material. As outlined below, the energy acceptor materials F8BT and 20F1/4F8BT could be modeled by including only singlet states, therefore the oscillator strength of the stimulated emission of the singlet exciton was readily available and determined to be $2.7 \cdot 10^{-17}$ and $1.7 \cdot 10^{-17}$ eV $\cdot$ Cm^2. For PFO, we for simplicity required the same oscillator strength α for both singlets and polarons, thereby assuming that the effective extension along the PFO chain is the same for an exciton and a polaron, and thus from S(10):

$$\alpha = \frac{\sum_i a_i(0)}{d \cdot c_{ph}} \qquad\qquad\qquad\qquad\qquad (EQ.\ S12)$$

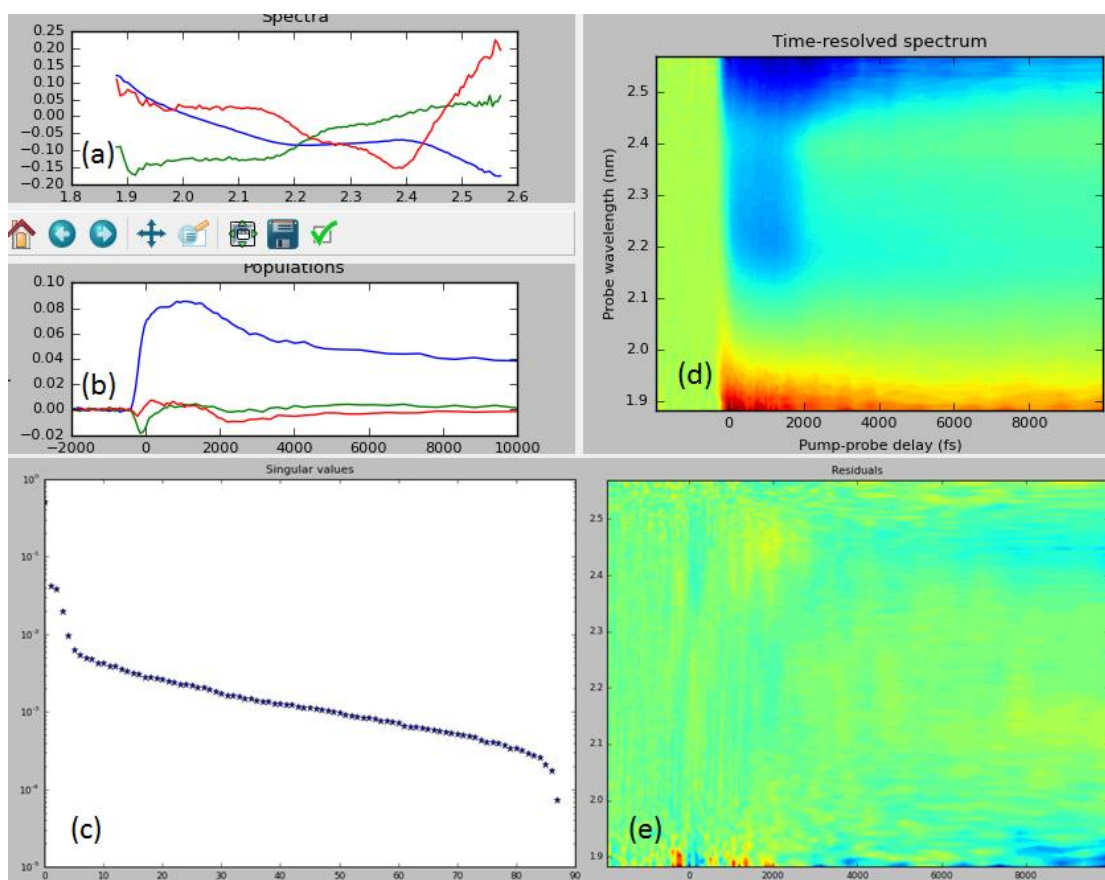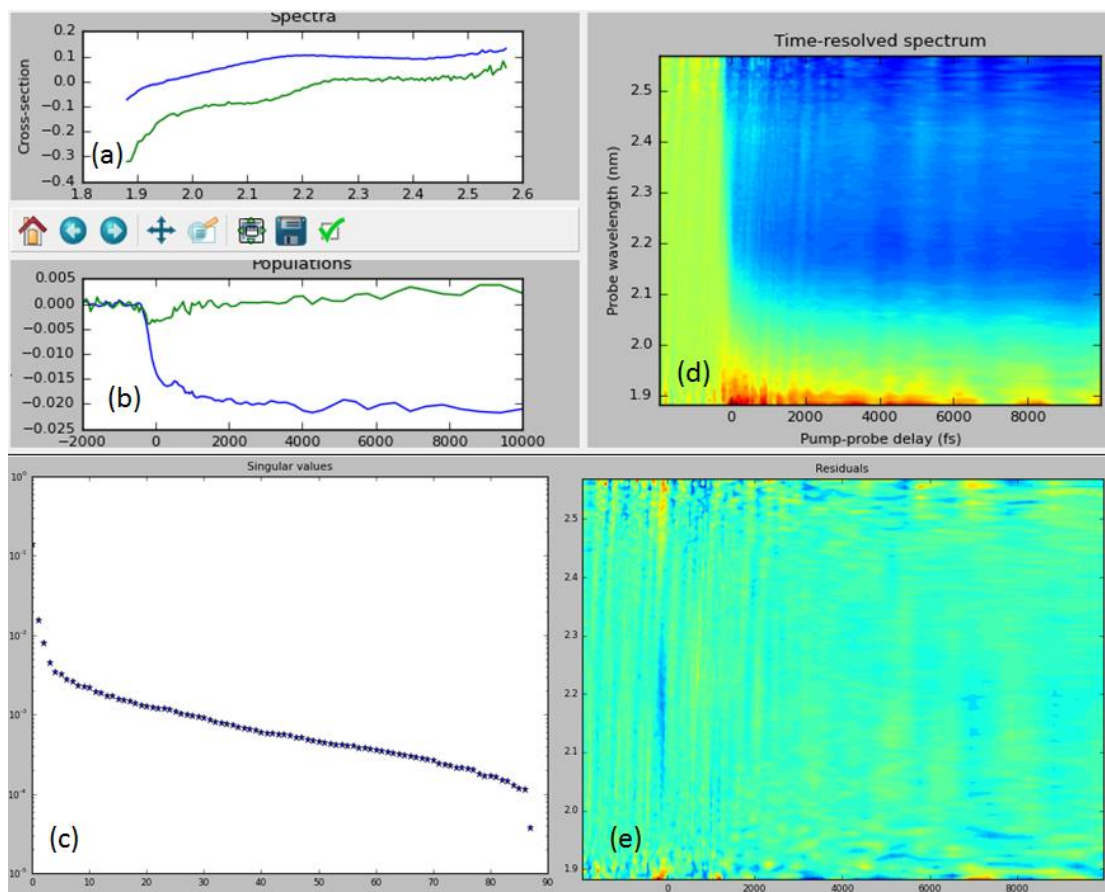we get $\alpha_{PFO} = 3.1 \cdot 10^{-17} eVcm^2$.
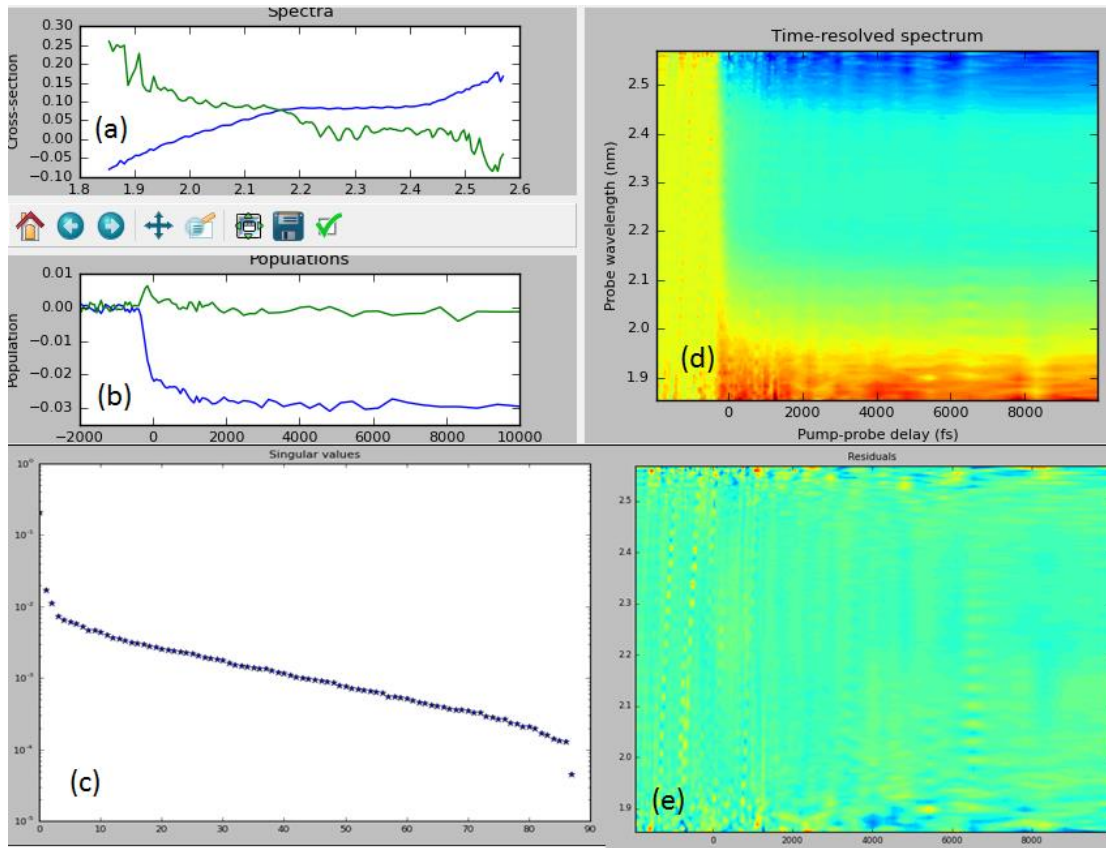
Figure S8. (**a**) Single value decomposition spectra, (**b**) populations, and (**c**) statistical weights of pristine F8BT films at low excitation intensity. (**d**) TA matrix and (**e**) residuals obtained using only two singular values are displayed in (**d**) and (**e**) respectively.
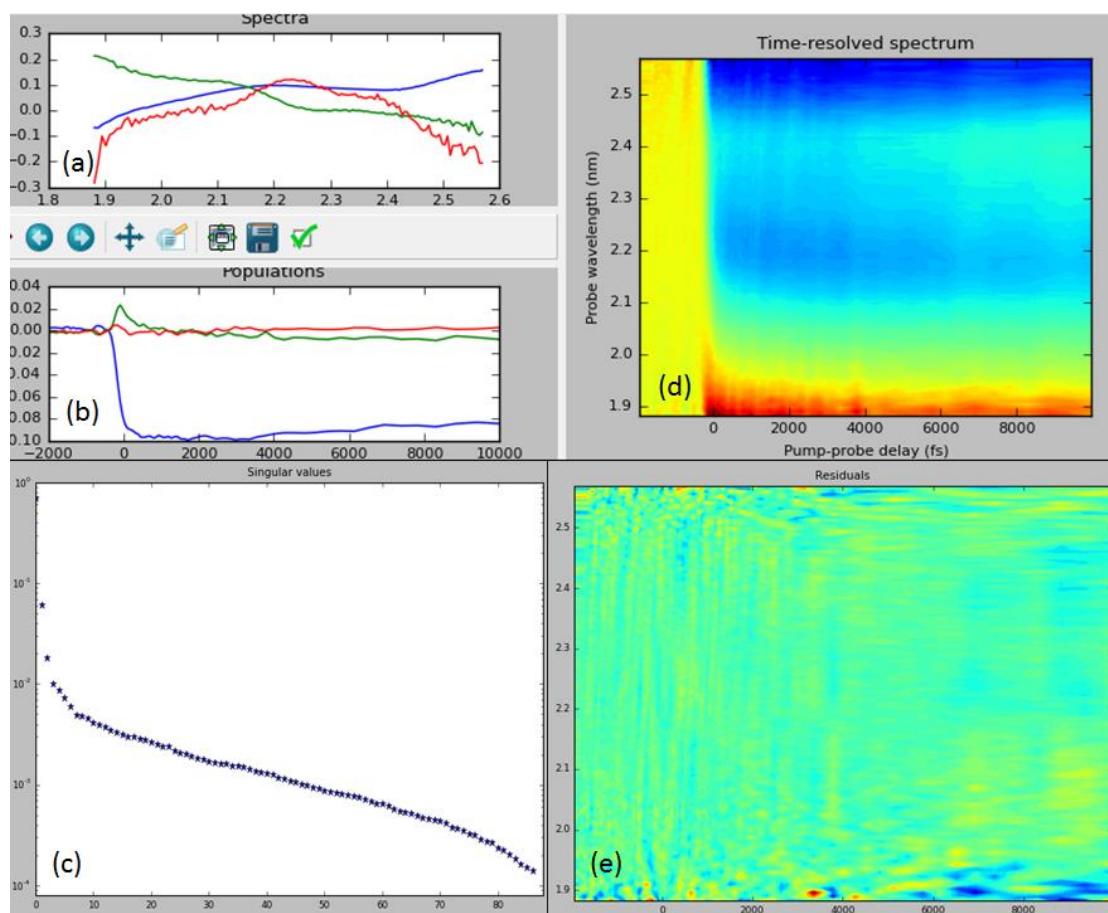
Figure S9. (**a**) Single value decomposition spectra, (**b**) populations, and (**c**) statistical weights of pristine F8BT films at high excitation intensity. (**d**) TA matrix and (**e**) residuals obtained using three singular values are displayed in (**d**) and (**e**) respectively.
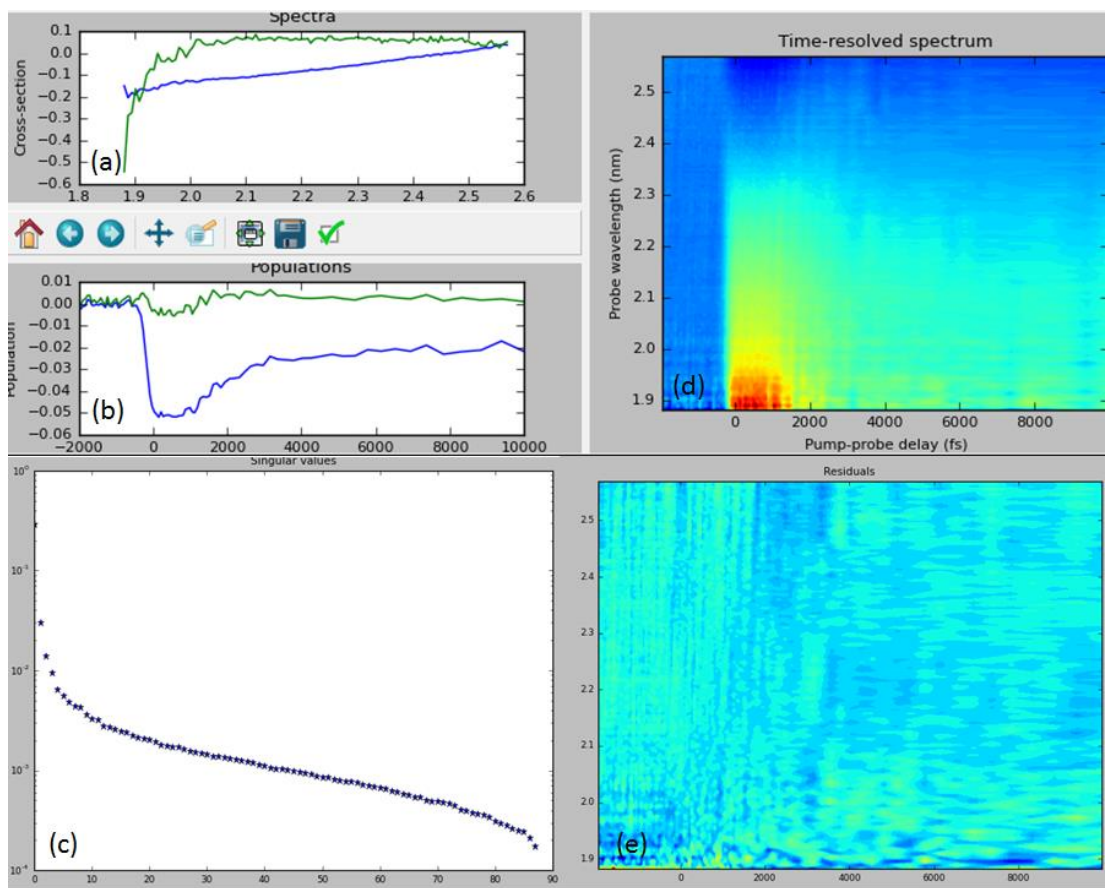
Figure S10. (**a**) Single value decomposition spectra, (**b**) populations, and (**c**) statistical weights of pristine 20F1/4F8BT films at low excitation intensity. (**d**) TA matrix and (**e**) residuals obtained using two singular values are displayed in (**d**) and (**e**) respectively.
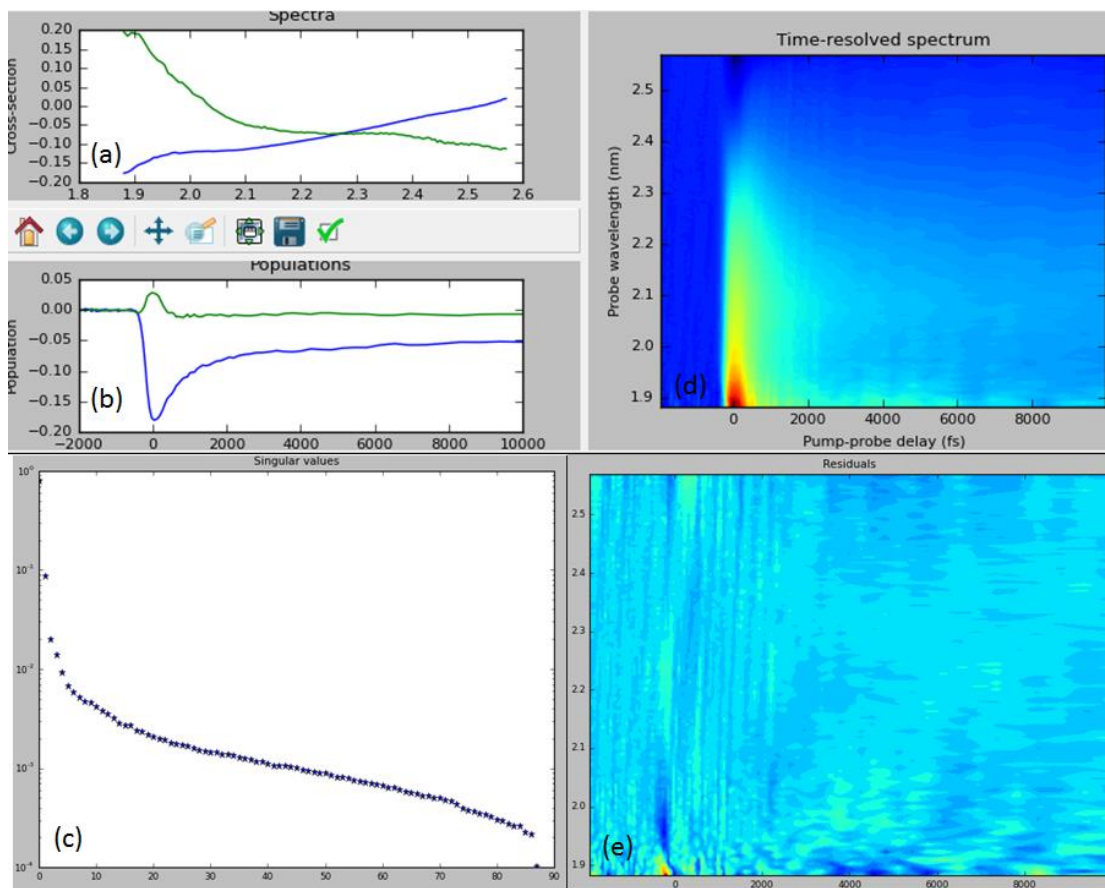
Figure S11. (**a**) Single value decomposition spectra, (**b**) populations, and (**c**) statistical weights of pristine 20F1/4F8BT films at high excitation intensity. (**d**) TA matrix and (**e**) residuals obtained using three singular values are displayed in (**d**) and (**e**) respectively.

Figure S12. (**a**) Single value decomposition spectra, (**b**) populations, and (**c**) statistical weights of pristine PFO films at low excitation intensity. (**d**) TA matrix and (**e**) residuals obtained using two singular values are displayed in (**d**) and (**e**) respectively.

Figure S13. (**a**) Single value decomposition spectra, (**b**) populations, and (**c**) statistical weights of pristine PFO films at high excitation intensity. (**d**) TA matrix and (**e**) residuals obtained using two singular values are displayed in (**d**) and (**e**) respectively.
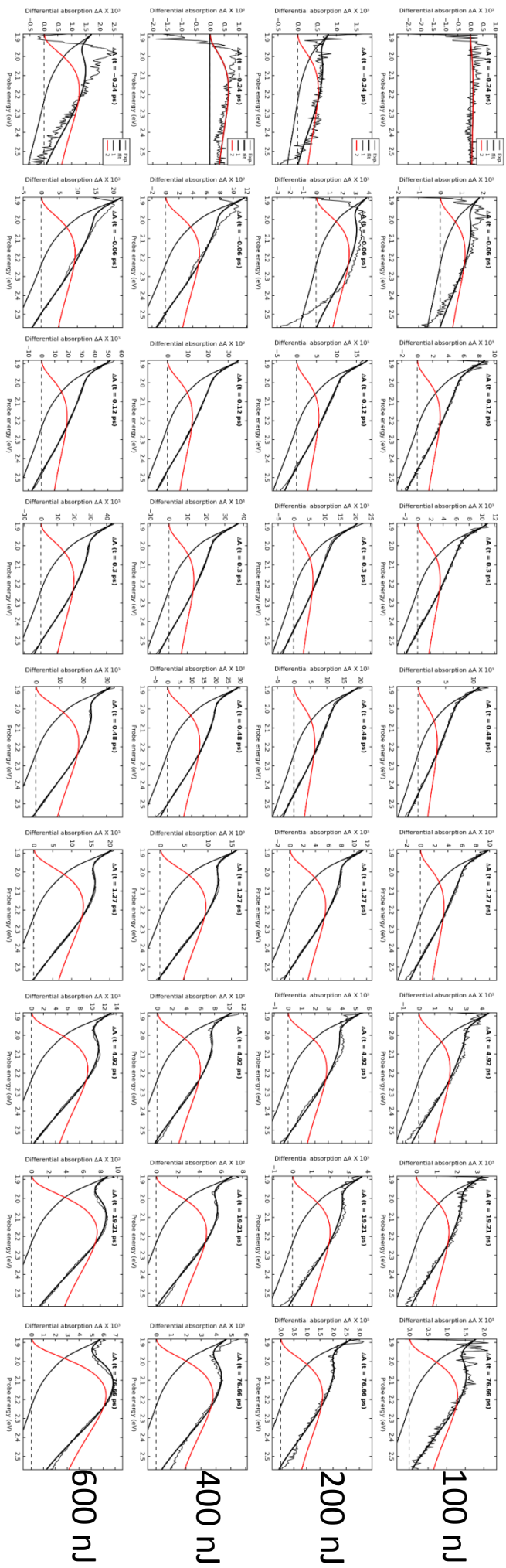
Figure S14. TA spectra of PFO (straight line) at different delay times and different excitation intensities and spectral fits (bold line) obtained with two excited states with cross-sections depicted by red and black straight lines, (ascribed to polaron-pairs and singlet excitons respectively).
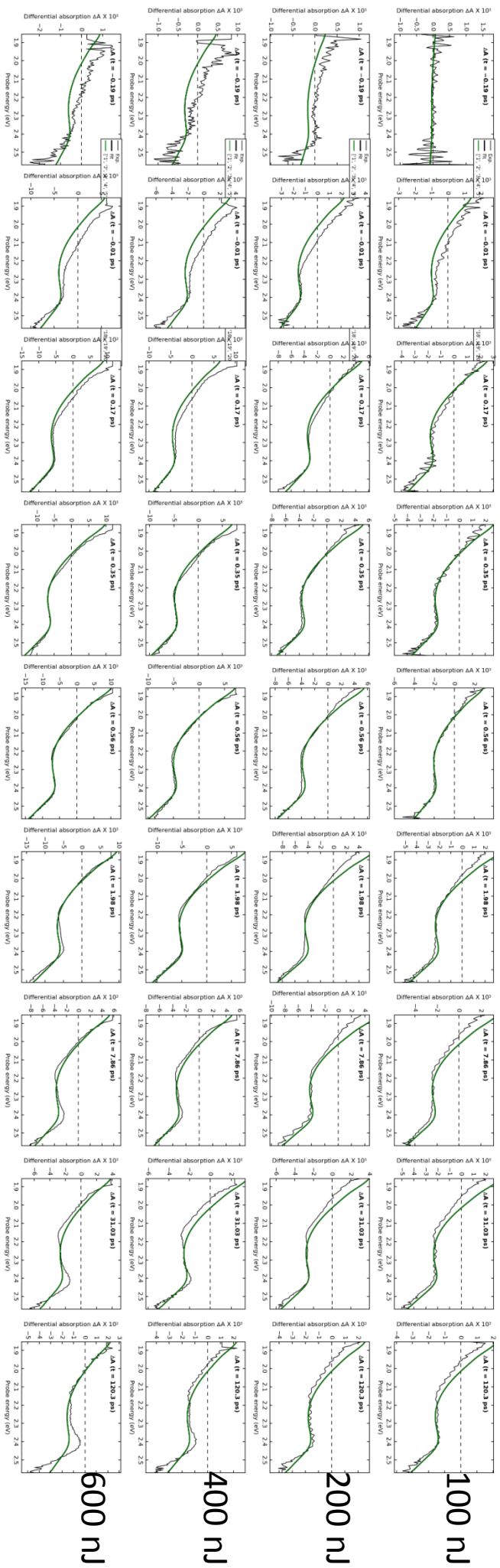
Figure S15. TA spectra of F8BT (straight line) at different delay times and different excitation intensities and spectral fit with one excited state with cross-section depicted as green bold line, (ascribed to singlet excitons).
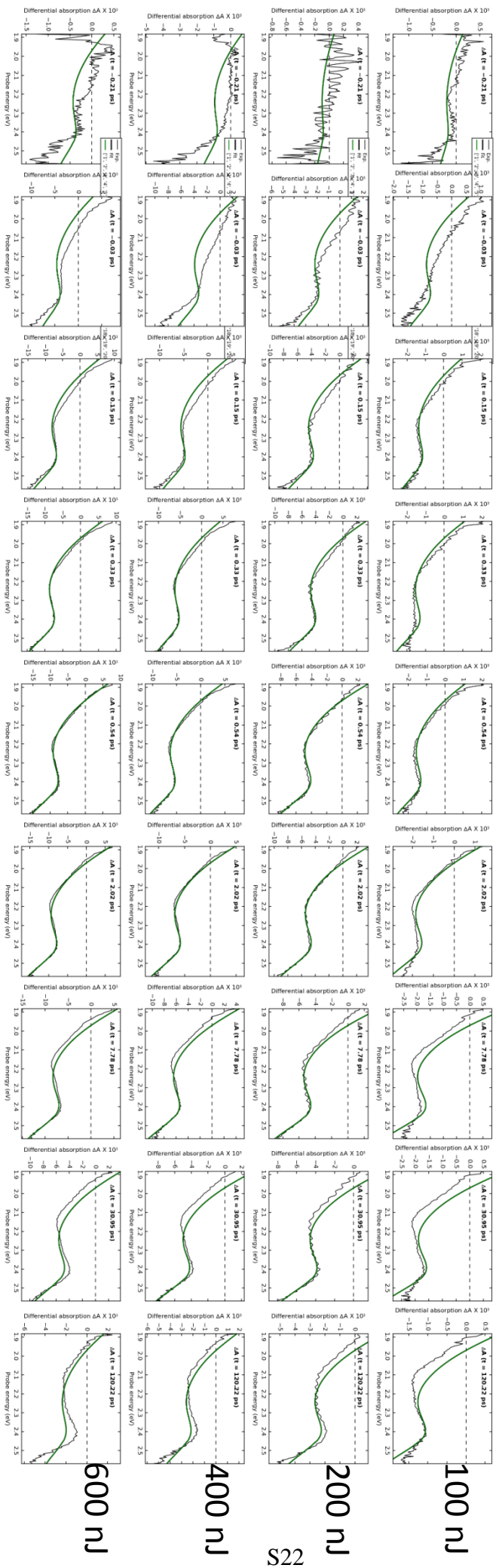
Figure S16. TA spectra of 20F1/4F8BT (straight line) at different delay times and different excitation intensities and spectral fit obtained with one excited state with cross-section depicted by green bold line, (ascribed to singlet excitons).
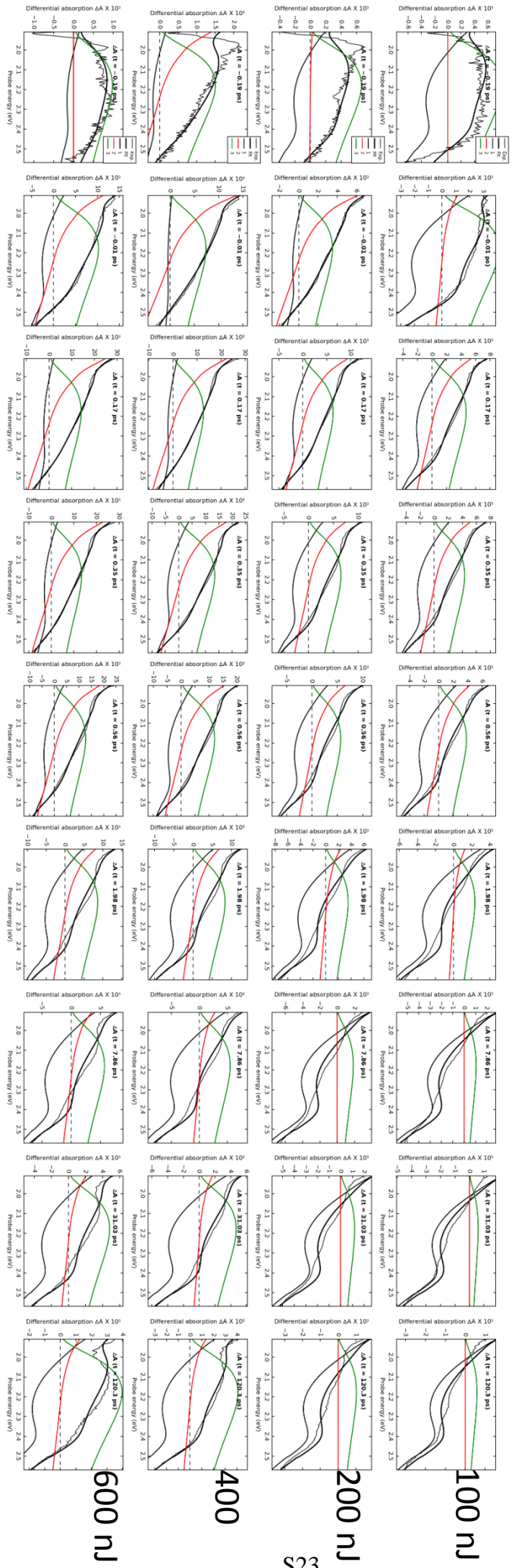
Figure S17. TA spectra of PFO:F8BT (straight line) at different delay times and different excitation intensities. Spectral fits (bold lines) were obtained employing three excited states with cross –sections associated to PFO singlet excitons and polaron-pairs (red and green lines) and F8BT singlet excitons (black straight line).
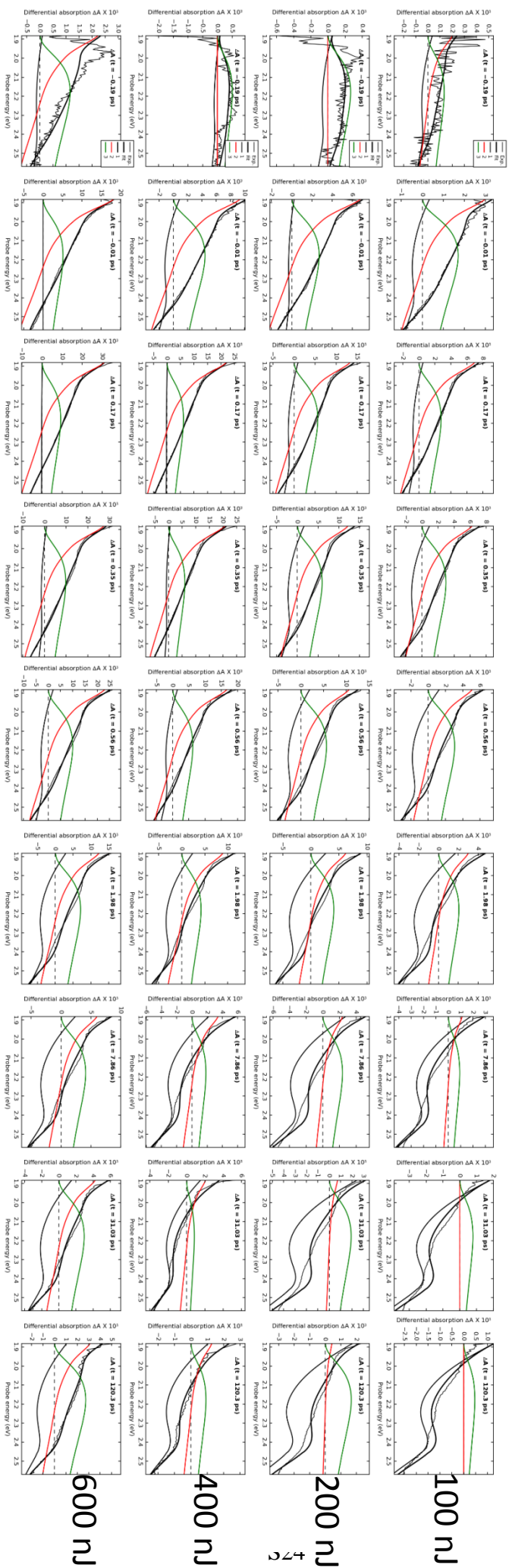
Figure S18. TA spectra of PFO:20F1/4F8BT (straight lines) at different delay times and different excitation intensities. Spectral fits (bold lines) were obtained employing three excited states with cross – sections associated to PFO singlets and polaron-pairs (red and green lines) and 20F1/4F8BT singlet excitons (black straight line).

[i]   Ivo H.M. van Stokkum, Delmar S. Larsen, Rienk van Grondelle, *Biochimica et Biophysica Acta*, **2004**, 1657, 82 – 104